Radiation Models for Thermal Flows at Low Mach Number

I. Teleaga[*], **M. Seaïd**[†], **I. Gasser**[‡], **A. Klar**[§], **J. Struckmeier**[¶]

Abstract

Simplified approximate models for radiation are proposed to study thermal effects in low Mach flow in open tunnels. The governing equations for fluid dynamics are derived by applying a low-Mach asymptotic in the compressible Navier-Stokes problem. Based on an asymptotic analysis we show that the integro-differential equation for radiative transfer can be replaced by a set of differential equations which are independent of angle variable and easy to solve using standard numerical discretizations. As an application we consider the situation of fires in vehicular tunnels. The results presented in this paper show that the proposed models are able to predict temperature in the tunnels accurately with low computational cost.

Keywords. Radiation hydrodymanics; low-Mach number flows; simplified P_N approximations; fires in vehicle tunnels.

1 Introduction

Thermal radiation in gas flows has direct effects on many industrial applications such as fires, furnaces and gas turbines. Growing concern with high temperature processes has emphasized the need for an evaluation of the effect of radiative heat transfer. Nevertheless, it is common for work on convective flows to neglect thermal radiation mainly because it involves tedious mathematics, which increase the computational work, and also because of the lack of detailed information on optical properties of the participating media and surfaces. However, radiation can strongly interact with convection in many situations of engineering interest and neglecting its effects may have significant consequences in the overall predictions. For discussion on the effect radiative properties of participating gases we refer to [9, 19, 10] and further references can be found therein.

The main difficulties raised when approximating thermal radiation in convection flows lie essentially on the large set of dependent unknowns and the coupling between the radiative transfer and the energy equation. The most accurate procedures available in the literature for computing radiation transfer in furnaces are the zonal and Monte Carlo methods [15]. However, these methods are not widely applied in comprehensive combustion calculations due to their large computational time and storage requirements. Also, the equations of the radiation transfer are in non-differential form, a significant inconvenience when solved in conjunction with the differential equations of flow

[*]Fachbereich Mathematik, Technische Universität Darmstadt, D–64289 Darmstadt, Germany (teleaga@mathematik.tu-darmstadt.de)

[†]Fachbereich Mathematik, Technische Universität Kaiserslautern, D–67663 Kaiserslautern, Germany (seaid@mathematik.uni-kl.de)

[‡]Fachbereich Mathematik, Technische Universität Hamburg, D–20146 Hamburg, Germany (gasser@math.uni-hamburg.de)

[§]Fachbereich Mathematik, Technische Universität Kaiserslautern, D–67663 Kaiserslautern, Germany (klar@itwm.fhg.de)

[¶]Fachbereich Mathematik, Technische Universität Hamburg, D–20146 Hamburg, Germany (struckmeier@math.uni-hamburg.de)

and convection. On the other hand, much of the current work on modeling energy transport in high-temperature gas or chemically reacting flows, uses computational fluid dynamics (CFD) codes. Therefore, the models for solving the radiative transfer equations must be compatible with the numerical method! s employed to solve the flow equations. The zonal and Monte Carlo methods for solving the radiative transfer problem are incompatible with the mathematical formulations used in CFD codes, and require prohibitive computational times for spatial resolution desired. The discrete ordinates methods [2] appear to be reasonable compromises for solving the radiative transfer equations, but still one has to deal with large systems of algebraic equations, resulting from discretizing angle and space coordinates, that may deteriorate the efficiency of the CFD solver. For these reasons, numerous investigations are currently being carried out worldwide to assess computationally efficient methods. The present work deals with the design of such methods.

In this paper, we consider the simplified P_N (SP_N) approximations to the radiation problem. The SP_N approximations were first proposed in [4] and theoretically studied in [12]. In [11, 18] the SP_N approximations have been extensively studied for radiative transfer in glass manufacturing, while in [3] they have been implemented for radiation in gas turbines. The SP_N approximations have also been studied in [1] for internal radiation in crystal growth. The main advantage in considering SP_N approximations is the fact that the radiative transfer equations are transformed to a set of parabolic/elliptic equations independent of the angular directions and easy to solve numerically using standard methods. Furthermore, comparisons presented in the above mentioned references have shown that the SP_N models approach the full radiative heat transfer with very low computational cost.

The motivation for this work is the need to obtain efficient numerical solutions to thermal radiation in gas flows at low Mach number. A typical example of such application is the modeling of fires in vehicle tunnels. As stated in [6, 5], the characteristic velocity in the tunnel is of order 1 m/s, for which low Mach number flow can be a suitable model. In fact, low Mach number approximation systematically removes acoustic waves without eliminating density variation. Here, the governing equations for unsteady compressible flow are the Navier-Stokes equations. For low Mach number flow, it is well known that numerical solution of these equations is computationally demanding because of the severe restriction imposed on the time step by acoustic wave propagation which is much faster than flow speeds. Following the work in [13], acoustic waves are removed by expanding independent variables in powers of the Mach number while density variations are still all! owed. When the essential dynamics in flows such as low-speed combustion is dependent on density differences but not compressibility (*e.g.* fire events in a tunnel) this procedure improves computational efficiency.

Compressibility effects can be neglected in low Mach number flows but density variations must still be accounted for when phenomena such as combustion are present. Then the time scale of acoustic waves is small compared to that of the hydrodynamic phenomena. An algorithm designed for general compressible flow will be computationally expensive because time steps must be small enough to resolve the acoustic waves while the integration period must remain large enough to capture the hydrodynamic phenomena. The radiation time-scale must be dealt with separately. Our goal in the present work is to develop robust and efficient solvers for the radiation convection problems. This is reached by coupling the low-Mach number flows for fluid dynamics and the SP_N models for the radiation. The coupled problem can be solved by a slight modification of the Marker and Cell (MAC) scheme [23, 7] for incompressible flows.

The layout of this paper is as follows. In section 2 we formulate the mathematical models for thermal flow and radiative transfer. This section includes the low-Mach asymptotic for the fluid dynamics and the SP_N approximation for the radiation transfer. Numerical solutions of the proposed models are presented in section 3. Section 4 is devoted to numerical results for two examples on fires in vehicular tunnels. Some concluding remarks are given in section 5.

2 Mathematical Equations

Modeling radiation hydrodynamics requires two sets of mathematical equations. The first set of equations models the fluid dynamics while the second set determines the radiative signal. The two processes have different physical characteristics and need careful numerical treatment, we refer to [14] for more details on radiation hydrodynamics. In this paper, a fluid dynamic model is derived using a low Mach asymptotic in the compressible Navier-Stokes equations whereas, the radiation model is formulated using an asymptotic expansion over an optical scale.

The compressible equations for conservation of mass, momentum and energy are

$$\begin{aligned} \partial_{\tilde{t}}\tilde{\rho} + \tilde{\nabla}\cdot(\tilde{\rho}\tilde{\mathbf{u}}) &= 0, \\ \tilde{\mathbf{u}}_{\tilde{t}} + (\tilde{\mathbf{u}}\cdot\tilde{\nabla})\tilde{\mathbf{u}} + \frac{1}{\tilde{\rho}}\tilde{\nabla}\tilde{p} &= \frac{\mu}{\tilde{\rho}}\left(\tilde{\Delta}\tilde{\mathbf{u}} + \frac{1}{3}\tilde{\nabla}(\tilde{\nabla}\cdot\tilde{\mathbf{u}})\right) + \tilde{\mathbf{f}}, \\ \partial_{\tilde{t}}\left(c_v\tilde{\rho}\tilde{T}\right) + \tilde{\nabla}\cdot\left(c_v\tilde{\mathbf{u}}\tilde{\rho}\tilde{T}\right) + \tilde{p}\tilde{\nabla}\tilde{\mathbf{u}} - \tilde{\nabla}\cdot\left(\lambda\tilde{\nabla}\tilde{T}\right) &= -\int_{\nu_0}^{\infty}\int_{\omega=4\pi}\tilde{\kappa}\left(\tilde{B}(\tilde{T},\nu) - \tilde{I}\right)d\omega d\nu + \tilde{q}, \end{aligned} \tag{2.1}$$

where $\tilde{\rho}(t,\mathbf{x})$, $\tilde{\mathbf{u}}(t,\mathbf{x})$, $\tilde{p}(t,\mathbf{x})$, $\tilde{T}(t,\mathbf{x})$ and $\tilde{I}(t,\nu,\omega,\mathbf{x})$ denote respectively the mass density, the flow velocity, the thermal pressure, the temperature of the fluid and the radiative intensity. Here $\mathbf{x}$ is the space coordinate, t the time variable, ω the directional angle and ν the frequency variable. The terms $\tilde{\mathbf{f}}$ and $\tilde{q}$ describe the external forces (*e.g.* gravitational force) and source contributions (*e.g.* heat or sink source), respectively. The quantities μ, λ, c_v are the dynamic viscosity, the heat conductivity and the specific heat coefficient at constant volume, respectively. The frequency ν_0 is the upper bound of opaque band of the optical spectrum where radiation is completely absorbed. By assuming that the fluid is a perfect gas, the fluid dynamic model is closed by the equation of state

$$\tilde{p} = R\tilde{\rho}\tilde{T}, \tag{2.2}$$

where $R = c_p - c_v$, with c_p is the specific heat coefficient at constant pressure. The spectral intensity $I(t,\nu,\omega,\mathbf{x})$ at time t, in position $\mathbf{x}$, within frequency ν and propagating along direction ω with a speed c, is obtained from the isotropic radiative transfer equation

$$\forall\nu > \nu_0: \qquad \frac{1}{c}\partial_{\tilde{t}}\tilde{I} + \omega\cdot\nabla\tilde{I} + (\tilde{\sigma}+\tilde{\kappa})\tilde{I} = \frac{\tilde{\sigma}}{4\pi}\int_{\omega=4\pi}\tilde{I}(t,\nu,\omega,\mathbf{x})d\omega + \tilde{\kappa}\tilde{B}(\tilde{T},\nu), \tag{2.3}$$

where $\tilde{\kappa}(\nu)$ is the absorption coefficient, $\tilde{\sigma}(\nu)$ is the scattering coefficient and $B(\tilde{T},\nu)$ is the spectral intensity of the black-body radiation given by the Planck function

$$\tilde{B}(\tilde{T},\nu) = \frac{2h\nu^3}{c_0^2}\left(e^{h\nu/k\tilde{T}} - 1\right)^{-1}, \tag{2.4}$$

with h, k and c_0 are Planck's constant, Boltzmann's constant and the speed of radiation propagation in vacuum, respectively, compare [14] for further physical details. For mathematical aspects of the radiative transfer equation and related issues see for instance [15]. Notice that in the above coupling we have assumed a thermodynamic equilibrium such that the fluid temperature and the radiation temperature are equal.

In order to rewrite the above equations in a dimensionless form, we define the following nondimensional variables

$$\begin{aligned} &\mathbf{x} = \frac{\tilde{\mathbf{x}}}{x_\infty}, \qquad t = \frac{\tilde{t}}{t_\infty}, \qquad \sigma = \frac{\tilde{\sigma}}{\sigma_\infty+\kappa_\infty}, \qquad \kappa = \frac{\tilde{\kappa}}{\sigma_\infty+\kappa_\infty}, \qquad \lambda = \frac{\tilde{\lambda}}{\lambda_\infty}, \\ &\rho = \frac{\tilde{\rho}}{\rho_\infty}, \qquad \mathbf{u} = \frac{\tilde{\mathbf{u}}}{u_\infty}, \qquad T = \frac{\tilde{T}}{T_\infty}, \qquad p = \frac{\tilde{p}}{p_\infty}, \qquad I = \frac{\tilde{I}}{I_\infty}, \end{aligned} \tag{2.5}$$

where the subscript "∞" represents reference quantities. We also impose the relations

$$t_\infty = \frac{x_\infty}{u_\infty}, \qquad p_\infty = R\rho_\infty T_\infty, \qquad I_\infty = c_v \rho_\infty T_\infty \mathbf{u}_\infty, \qquad B(T,\nu) = \frac{\tilde{B}(\tilde{T},\nu)}{I_\infty}. \tag{2.6}$$

Using the new variables (2.5), equations (2.1) can be rewritten in dimensionless as

$$\begin{aligned} \partial_t \rho + \nabla \cdot (\rho \mathbf{u}) &= 0, \\ \partial_t \mathbf{u} + \mathbf{u} \cdot \nabla \mathbf{u} + \frac{1}{\gamma M^2}\frac{1}{\rho}\nabla p - \frac{1}{Re}\frac{1}{\rho}\left(\Delta \mathbf{u} + \frac{1}{3}\nabla(\nabla \cdot \mathbf{u})\right) &= \mathbf{f}, \\ \partial_t (\rho T) + \nabla \cdot (\mathbf{u}\rho T) + (\gamma - 1) p \nabla \cdot \mathbf{u} - \frac{\gamma}{Pr}\frac{1}{Re}\Delta T &= -\frac{1}{\tau}\int_{\nu_0}^{\infty} \kappa\big(4\pi B(T,\nu) - \varphi\big) d\nu + q, \end{aligned} \tag{2.7}$$

where the adiabatic exponent γ, the Mach number M, the Reynolds number Re, the Prandtl number Pr and the Froude number Fr are given by

$$\gamma = \frac{c_p}{c_v}, \qquad M^2 = \frac{\rho_\infty u_\infty^2}{\gamma p_\infty}, \qquad Re = \frac{\rho_\infty u_\infty x_\infty}{\mu}, \qquad Pr = \frac{\mu c_p}{\lambda}, \qquad Fr = \frac{u_\infty}{\sqrt{x_\infty \|\mathbf{f}\|}}, \tag{2.8}$$

with

$$\mathbf{f} = \frac{\tilde{\mathbf{f}}}{Fr^2 \|\tilde{\mathbf{f}}\|}, \qquad q = \frac{q_\infty x_\infty}{u_\infty p_\infty}(\gamma - 1)\tilde{q}.$$

For the situation of fires in vehicular tunnels, typical values for the reference parameters and the dimensionless numbers (2.8) can be found in [6]. In the equations (2.7), φ is the total incident radiation defined as

$$\varphi(t,\nu,\mathbf{x}) = \int_{\omega=4\pi} I(t,\nu,\omega,\mathbf{x}) d\omega. \tag{2.9}$$

Analogously, the radiative transfer equation (2.3) can be rewritten in dimensionless as

$$\forall \nu > \nu_0 : \quad \frac{1}{c}\partial_t I + \tau\omega \cdot \nabla I + (\sigma + \kappa) I = \frac{\sigma}{4\pi}\varphi + \kappa B(T,\nu), \tag{2.10}$$

where the optical scale τ is defined by

$$\tau = \frac{1}{(\sigma_\infty + \kappa_\infty) x_\infty}. \tag{2.11}$$

Note that the scaling parameter τ depends on optical characteristics of the fluid and reference height of the fluid domain. It can be viewed as a dimensionless number to differentiate between an optically thick medium ($\tau \ll 1$) and an optically thin medium ($\tau \approx 1$).

Equations (2.7) and (2.10) have to be solved in a bounded domain Ω with smooth boundary $\partial\Omega$ and subject to given initial and boundary conditions. These conditions strongly depend on the problem under consideration. Since the emphasis in the present work is to simulate fires in vehicular tunnels, we shall focus in a generic two-dimensional tunnel shown in figure 1, and boundary conditions are set according to its geometry. Thus

$$\partial\Omega = \Gamma_1 \cup \Gamma_2 \cup \Gamma_3 \cup \Gamma_4, \tag{2.12}$$

where Γ_1 and Γ_2 represent the entrance and exit of the tunnel, while α defines the tunnel slope.

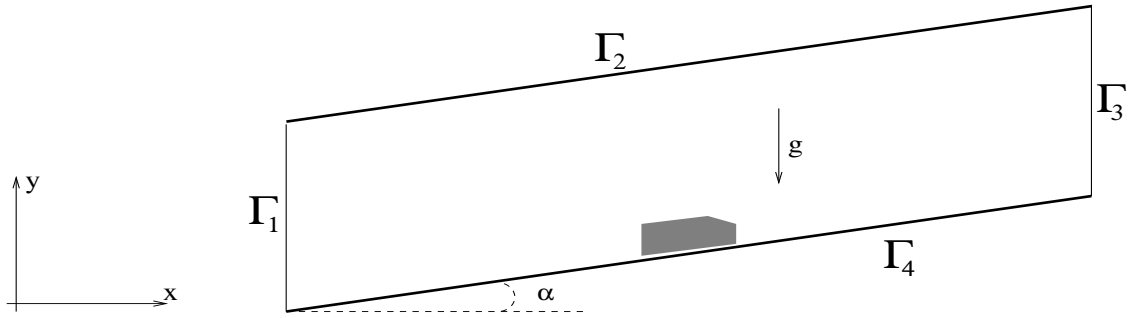

Figure 1: A generic two-dimensional domain for vehicular tunnels.

2.1 Low Mach Asymptotics

There are two approaches for solving low Mach number flows. The first approach begins with the equations for compressible flow, devise a numerical method and then consider modifications to the numerical algorithm when low Mach number flows are encountered. In practice, this procedure is performed using some type of preconditioning techniques in the sense that they scale the eigenvalues of the system to similar orders of magnitude and remove the disparity in wave speeds, leading to a well-conditioned system, compare for instance [21]. The second approach is to begin with the equations for low Mach number flows and adapt numerical schemes devised for incompressible flows to allow density variations. This last approach has been taken here.

The approach consists in a Taylor series expansion of variables (in our case the pressure) in power terms of the Mach number. The basic idea behind this technique is to decrease the numerical representation of the speed of sound artificially, by subtracting a constant pressure $p^{(0)}$ across the entire domain,

$$p = p^{(0)} + \epsilon p^{(1)} + \mathcal{O}(\epsilon^2), \tag{2.13}$$

where $\epsilon = \gamma M^2$, $p^{(0)}$ is the ground pressure and $p^{(1)}$ is the fluctuation pressure part. The leading order momentum equation reduces to $\nabla p^{(0)} = 0$; therefore, $p^{(0)}$ can only be a function of time *i.e.* $p^{(0)} = p^{(0)}(t)$. In closed systems, the ground pressure may change with time whereas it remains constant in open systems like vehicular tunnels considered in this paper. Then, considering $p^{(0)} = constant$ and that in leading order we have $T = p^{(0)}/\rho$, the system (2.7) can be rewritten as

$$\begin{aligned} \partial_t \rho + \nabla \cdot (\rho \mathbf{u}) &= 0, \\ \partial_t \mathbf{u} + (\mathbf{u} \cdot \nabla)\mathbf{u} + \frac{1}{\rho}\nabla p &= \frac{1}{Re}\frac{1}{\rho}\left(\Delta \mathbf{u} + \frac{1}{3}\nabla(\nabla \cdot \mathbf{u})\right) + \mathbf{f}, \\ \nabla \cdot \mathbf{u} &= Q, \end{aligned} \tag{2.14}$$

where the right-hand side term Q is given by

$$Q(T,\varphi) = \frac{1}{p^{(0)}\, Pr\, Re}\Delta T - \frac{1}{\gamma p^{(0)}}\frac{1}{\tau}\int_{\nu_0}^{\infty} \kappa\big(4\pi B(T,\nu) - \varphi\big)d\nu + \frac{q}{\gamma p^{(0)}}, \qquad T = \frac{p^{(0)}}{\rho}.$$

Note that all quantities that appear in these equations, are the leading order terms (ϵ^0) of their corresponding expansion, except for the hydrodynamic pressure $p = p^{(1)}$, which appears in the momentum equation and is a first order (ϵ^1) quantity. The nonlinear system (2.14) is transformed

using a modified projection method described in [5] into

$$\begin{aligned} \partial_t \rho + \nabla \cdot (\rho \mathbf{u}) &= 0, \\ \partial_t \mathbf{u} + (\mathbf{u} \cdot \nabla)\mathbf{u} + \frac{1}{\rho}\nabla p &= \frac{1}{Re}\frac{1}{\rho}\left(\Delta \mathbf{u} + \frac{1}{3}\nabla Q\right) + \mathbf{f}, \\ \nabla \cdot \left(\frac{1}{\rho}\nabla p\right) &= \nabla \cdot \left(\frac{1}{Re}\frac{1}{\rho}\left(\Delta \mathbf{u} + \frac{1}{3}\nabla Q\right) + \mathbf{f}\right). \end{aligned} \tag{2.15}$$

For the above system we impose the following boundary conditions

$$\begin{aligned} \mathbf{n}(\hat{\mathbf{x}}) \cdot \nabla \mathbf{u}(t, \hat{\mathbf{x}}) &= 0, \qquad \forall\, \hat{\mathbf{x}} \in \Gamma_1 \cup \Gamma_3, \\ \mathbf{u}(t, \hat{\mathbf{x}}) &= 0, \qquad \forall\, \hat{\mathbf{x}} \in \Gamma_2 \cup \Gamma_4, \\ \rho(t, \hat{\mathbf{x}}) &= \rho_0, \qquad \forall\, \hat{\mathbf{x}} \in \Gamma_1^-, \\ \rho(t, \hat{\mathbf{x}}) &= \rho_1, \qquad \forall\, \hat{\mathbf{x}} \in \Gamma_3^-, \\ p(t, \hat{\mathbf{x}}) &= p_0, \qquad \forall\, \hat{\mathbf{x}} \in \Gamma_1, \\ p(t, \hat{\mathbf{x}}) &= p_1, \qquad \forall\, \hat{\mathbf{x}} \in \Gamma_3, \\ \mathbf{n}(\hat{\mathbf{x}}) \cdot \nabla p(t, \hat{\mathbf{x}}) &= \frac{1}{Re}\frac{1}{\rho}\left(\Delta \mathbf{u} + \frac{1}{3}\nabla Q\right) \cdot \mathbf{n}(\hat{\mathbf{x}}) + \mathbf{f} \cdot \mathbf{n}(\hat{\mathbf{x}}), \qquad \forall\, \hat{\mathbf{x}} \in \Gamma_2 \cup \Gamma_4, \end{aligned} \tag{2.16}$$

where $\mathbf{n}(\hat{\mathbf{x}})$ denotes the outward normal in $\hat{\mathbf{x}}$ with respect to $\partial\Omega$ and

$$\Gamma_1^- = \{\hat{\mathbf{x}} \in \Gamma_1 : \quad \mathbf{n}(\hat{\mathbf{x}}) \cdot \mathbf{u}(t, \hat{\mathbf{x}}) \leq 0\}, \qquad \Gamma_3^- = \{\hat{\mathbf{x}} \in \Gamma_3 : \quad \mathbf{n}(\hat{\mathbf{x}}) \cdot \mathbf{u}(t, \hat{\mathbf{x}}) \leq 0\}.$$

As pointed out in [5], using Dirichlet boundary conditions for pressure at the ends of the domain we can directly simulate atmospheric effects or the pressure induced by ventilators. It is known that a ventilator produces an over pressure which induces a certain velocity to the fluid.

2.2 Simplified P_N Approximations

The SP_N approximations for radiative heat transfer problems have been analyzed in [11]. The SP_N approximations have also been studied in [18, 8] for glass manufacturing and in [3] for gas turbines. Here we extend these approximations to the radiation hydrodynamics. Since the photons travel with very high speed, the term $1/c$ in (2.10) is negligible and is dropped in the remainder of paper.

First we rewrite the equation (2.10) as

$$\left(1 + \frac{\tau}{\sigma + \kappa}\omega \cdot \nabla\right) I = S,$$

where the right-hand term is given by

$$S = \frac{1}{\sigma + \kappa}\left(\frac{\sigma}{4\pi}\varphi + \kappa B(T, \nu)\right).$$

Then, we apply a Neumann series to formally invert the transport operator

$$\begin{aligned} I &= \left(1 + \frac{\tau}{\sigma + \kappa}\omega \cdot \nabla\right)^{-1} S \\ &\approx \left(1 - \frac{\tau}{\sigma + \kappa}\omega \cdot \nabla + \frac{\tau^2}{(\sigma + \kappa)^2}(\omega \cdot \nabla)^2 - \frac{\tau^3}{(\sigma + \kappa)^3}(\omega \cdot \nabla)^3 + \cdots\right) S. \end{aligned}$$

Note that the source term S does not depend of the angle coordinates. Integrating respect to ω over all directions in the unit sphere and using

$$\int_{\omega = 4\pi} (\omega \cdot \nabla)^n d\omega = \left(1 + (-1)^n\right)\frac{2\pi}{n+1}\nabla^n,$$

with $\nabla^2 = \nabla \cdot \nabla = \Delta$, we obtain the formal asymptotic equation for φ

$$4\pi S = \left(1 - \frac{\tau^2}{3(\sigma+\kappa)^2}\nabla^2 - \frac{4\tau^4}{45(\sigma+\kappa)^4}\nabla^4 - \frac{44\tau^6}{945(\sigma+\kappa)^6}\nabla^6\right)\varphi + \mathcal{O}(\tau^8).$$

When terms of $\mathcal{O}(\tau^2)$, $\mathcal{O}(\tau^4)$, $\mathcal{O}(\tau^6)$ or $\mathcal{O}(\tau^8)$ are neglected we obtain the SP_0, SP_1, SP_2 or SP_3 approximations, respectively. Higher order approximations can be derived in a similar manner.

The SP_0 approximation:

$$\varphi = 4\pi S,$$

which is equivalent to

$$\forall\ \nu > \nu_0 : \qquad \varphi = 4\pi B(T,\nu). \tag{2.17}$$

Note that the equilibrium (2.17) cancels the radiation effects in the fluid dynamics model (2.7). In this paper, we consider only the SP_1 and SP_3 approximations and our techniques can be straightforwardly extended to other approximations. Thus,

The SP_1 approximation:

$$4\pi S = \varphi - \frac{\tau^2}{3(\sigma+\kappa)^2}\nabla^2\varphi + \mathcal{O}(\tau^4),$$

and the associated equations are given by

$$\forall\ \nu > \nu_0 : \qquad -\frac{\tau^2}{3\,(\sigma+\kappa)}\Delta\varphi + \kappa\varphi = 4\pi\kappa B(T,\nu). \tag{2.18}$$

The SP_3 approximation:

$$4\pi S = \left(1 - \frac{\tau^2}{3(\sigma+\kappa)^2}\nabla^2 - \frac{4\tau^4}{45(\sigma+\kappa)^4}\nabla^4 - \frac{44\tau^6}{945(\sigma+\kappa)^6}\nabla^6\right)\varphi + \mathcal{O}(\tau^8),$$

and the associated equations are given by

$$\begin{aligned} \forall\ \nu > \nu_0 : \qquad -\frac{\tau^2}{\sigma+\kappa}\mu_1^2\Delta\psi_1 + \kappa\psi_1 &= 4\pi\kappa B(T,\nu), \\ -\frac{\tau^2}{\sigma+\kappa}\mu_2^2\Delta\psi_2 + \kappa\psi_2 &= 4\pi\kappa B(T,\nu). \end{aligned} \tag{2.19}$$

The new variables ψ_1 and ψ_2 in (2.19) are related to the total incident intensity (2.9) by the relation

$$\varphi = \frac{\gamma_2\psi_1 - \gamma_1\psi_2}{\gamma_2 - \gamma_1}. \tag{2.20}$$

The boundary conditions for $\mathrm{SP_N}$ approximations are derived from variational principles and are strongly connected to the $\mathrm{P_N}$ approximations Marshak's conditions, compare [15]. Here we formulate boundary conditions for the $\mathrm{SP_N}$ approximations which are consistent with fluid boundary conditions (2.16). For more general formulation of these boundary conditions we refer the reader to [11]. Hence, the boundary conditions for SP_1 equations (2.18) are

$$\begin{aligned} \mathbf{n}(\hat{\mathbf{x}})\cdot\nabla\varphi(t,\hat{\mathbf{x}}) &= 0, \qquad \forall\,\hat{\mathbf{x}} \in \Gamma_2 \cup \Gamma_4, \\ \frac{\tau}{3(\sigma+\kappa)}\mathbf{n}(\hat{\mathbf{x}})\cdot\nabla\varphi(t,\hat{\mathbf{x}}) + \varphi(t,\hat{\mathbf{x}}) &= 4\pi B\left(T(t,\hat{\mathbf{x}}),\nu\right), \qquad \forall\,\hat{\mathbf{x}} \in \Gamma_1^- \cup \Gamma_3^-. \end{aligned} \tag{2.21}$$

For SP_3 equations (2.19), the boundary conditions are given by

$$\begin{aligned}
\mathbf{n}(\hat{\mathbf{x}})\cdot\nabla\psi_1(t,\hat{\mathbf{x}}) &= 0, \quad \mathbf{n}(\hat{\mathbf{x}})\cdot\nabla\psi_2(t,\hat{\mathbf{x}})=0, \qquad \forall\,\hat{\mathbf{x}}\in\Gamma_2\cup\Gamma_4,\\
\frac{\tau}{\sigma+\kappa}\mathbf{n}(\hat{\mathbf{x}})\cdot\nabla\psi_1(t,\hat{\mathbf{x}})+\alpha_1\psi_1(t,\hat{\mathbf{x}}) &= \eta_1 B\left(T(t,\hat{\mathbf{x}}),\nu\right)+\beta_2\psi_2(t,\hat{\mathbf{x}}), \quad \forall\,\hat{\mathbf{x}}\in\Gamma_1^-\cup\Gamma_3^-,\\
\frac{\tau}{\sigma+\kappa}\mathbf{n}(\hat{\mathbf{x}})\cdot\nabla\psi_2(t,\hat{\mathbf{x}})+\alpha_2\psi_2(t,\hat{\mathbf{x}}) &= \eta_2 B\left(T(t,\hat{\mathbf{x}}),\nu\right)+\beta_1\psi_1(t,\hat{\mathbf{x}}), \quad \forall\,\hat{\mathbf{x}}\in\Gamma_1^-\cup\Gamma_3^-.
\end{aligned} \tag{2.22}$$

According to (2.16), the boundary temperature $T(t,\hat{\mathbf{x}})$ in (2.21) and (2.22) is defined as

$$T(t,\hat{\mathbf{x}})=\begin{cases}\dfrac{p_0}{\rho_0}, & \text{if} \quad \hat{\mathbf{x}}\in\Gamma_1^-,\\[2ex] \dfrac{p_0}{\rho_1}, & \text{if} \quad \hat{\mathbf{x}}\in\Gamma_3^-.\end{cases}$$

The remaining parameters appeared in (2.19), (2.20) and (2.22) are listed as follows:

$$\begin{aligned}
&\mu_1^2=0.11558711, \quad \mu_2^2=0.74155574, \qquad \gamma_1=-1.6330966, \quad \gamma_2=3.0616681,\\
&\alpha_1=2.06453963, \quad \alpha_2=1.28268259, \qquad \beta_1=-0.28678023, \quad \beta_2=0.300669118,\\
&\eta_1=29.7220898, \qquad \eta_2=12.5148781.
\end{aligned}$$

It is noteworthy that these parameters are valid only when non-reflective boundary conditions are supplied to the radiative transfer equation (2.3). In [11], mathematical formulae to handle more general boundary conditions in (2.3) are given.

3 Solution Procedure

The fluid dynamics and radiation equations presented in the previous section can be solved using existing codes from computational fluid dynamics. In the current work, the fluid flow equations (2.15)-(2.16) are solved by a modified projection method based on the MAC scheme. This method is similar to that used in [5] as an extension of the MAC scheme [23] for incompressible flows. The essential differences are in use of extra source term and the inclusion of radiation effects. The SP_N equations (2.18) and (2.21), or (2.19) and (2.22) are solved using a central difference scheme using the same mesh hierarchy as the one used in fluid dynamics solution.

Let us consider the two-dimensional case *i.e.*, $\mathbf{x}=(x,y)$, $\mathbf{u}=(u,v)$ and $\mathbf{f}=(f_1,f_2)$. The time interval is divided into subintervals $[t_n,t_{n+1}]$ with $t_n=n\Delta t$ and let w^n denotes the value of an arbitrary function w at time t_n. Given $\{p^n,\rho^n,u^n,v^n,T^n,\varphi^n\}$, we compute the solution $\left\{p^{n+1},\rho^{n+1},u^{n+1},v^{n+1},T^{n+1},\varphi^{n+1}\right\}$ as follows:

Step 1. Solve for φ^{n+1}

$$\forall\ \nu>\nu_0: \qquad -\frac{\tau^2}{3\left(\sigma+\kappa\right)}\Delta\varphi^{n+1}+\kappa\varphi^{n+1}=4\pi\kappa B(T^n,\nu), \tag{3.1}$$

in case of SP_1 approximation or

$$\begin{aligned}
\forall\ \nu>\nu_0: \qquad -\frac{\tau^2}{\sigma+\kappa}\mu_1^2\Delta\psi_1^{n+1}+\kappa\psi_1^{n+1} &= 4\pi\kappa B(T^n,\nu),\\
-\frac{\tau^2}{\sigma+\kappa}\mu_2^2\Delta\psi_2^{n+1}+\kappa\psi_2^{n+1} &= 4\pi\kappa B(T^n,\nu),
\end{aligned} \tag{3.2}$$

$$\varphi^{n+1} = \frac{\gamma_2 \psi_1^{n+1} - \gamma_1 \psi_2^{n+1}}{\gamma_2 - \gamma_1}, \tag{3.3}$$

in case of SP_3 approximation.

Step 2. Formulate the intermediate source term $Q^{n+1/2}$

$$Q^{n+1/2} = \frac{1}{p_0\, Pr\, Re}\Delta T^n - \frac{1}{\gamma p_0}\frac{1}{\tau}\int_{\nu_0}^{\infty} \kappa \left(4\pi B(T^n, \nu) - \varphi^{n+1}\right) d\nu + \frac{q}{\gamma p_0}. \tag{3.4}$$

Step 3. Update the density ρ^{n+1}

$$\frac{\rho^{n+1} - \rho^n}{\Delta t} + u^n \frac{\partial \rho^n}{\partial x} + v^n \frac{\partial \rho^n}{\partial y} + \rho^n Q^{n+1/2} = 0. \tag{3.5}$$

Step 4. Update the temperature T^{n+1}

$$T^{n+1} = \frac{p_0}{\rho^{n+1}}. \tag{3.6}$$

Step 5. Formulate the source term Q^{n+1}

$$Q^{n+1} = \frac{1}{p_0\, Pr\, Re}\Delta T^{n+1} - \frac{1}{\gamma p_0}\frac{1}{\tau}\int_{\nu_0}^{\infty} \kappa \left(4\pi B(T^{n+1}, \nu) - \varphi^{n+1}\right) d\nu + \frac{q}{\gamma p_0}. \tag{3.7}$$

Step 6. Calculate an auxiliary velocity (u^{aux}, v^{aux})

$$\begin{aligned}
\frac{u^{aux} - u^n}{\Delta t} + \frac{\partial (u^n)^2}{\partial x} + \frac{\partial u^n v^n}{\partial y} - u^n Q^{n+1} - \frac{1}{Re}\frac{1}{\rho^{n+1}}\left(\Delta u^n + \frac{1}{3}\frac{\partial Q^{n+1}}{\partial x}\right) &= f_1^n, \\
\frac{v^{aux} - v^n}{\Delta t} + \frac{\partial u^n v^n}{\partial x} + \frac{\partial (v^n)^2}{\partial y} - v^n Q^{n+1} - \frac{1}{Re}\frac{1}{\rho^{n+1}}\left(\Delta v^n + \frac{1}{3}\frac{\partial Q^{n+1}}{\partial y}\right) &= f_2^n.
\end{aligned} \tag{3.8}$$

Step 7. Solve for the pressure p^{n+1}

$$-\frac{\partial}{\partial x}\left(\frac{\Delta t}{\rho^{n+1}}\frac{\partial p^{n+1}}{\partial x}\right) - \frac{\partial}{\partial y}\left(\frac{\Delta t}{\rho^{n+1}}\frac{\partial p^{n+1}}{\partial y}\right) = Q^{n+1} - \frac{\partial u^{aux}}{\partial x} - \frac{\partial v^{aux}}{\partial y}. \tag{3.9}$$

Step 8. Update the velocity $\left(u^{n+1}, v^{n+1}\right)$

$$\begin{aligned}
u^{n+1} &= u^{aux} - \frac{\Delta t}{\rho^{n+1}}\frac{\partial p^{n+1}}{\partial x}, \\
v^{n+1} &= v^{aux} - \frac{\Delta t}{\rho^{n+1}}\frac{\partial p^{n+1}}{\partial y}.
\end{aligned} \tag{3.10}$$

Note that the Poisson problem (3.9) is obtained by taking the divergence of equations (3.8) and using the fact that $\nabla \cdot \mathbf{u} = Q$. In the solution procedure, two linear systems have to be solved at each time step to update the total incident radiation φ^{n+1} from (3.1) or (3.2) and the pressure p^{n+1} from (3.9). To solve these linear systems in our algorithm we have implemented a preconditioned conjugate gradient from [22].

The discretization of spatial derivatives appeared in above steps, is carried out using a staggered grid in which the different variables are approximated at different gridpoints as shown in figure 2. This type of meshes, widely used in computational fluid dynamics, guarantees that the computed flow solution is not perturbed by spurious pressure modes.

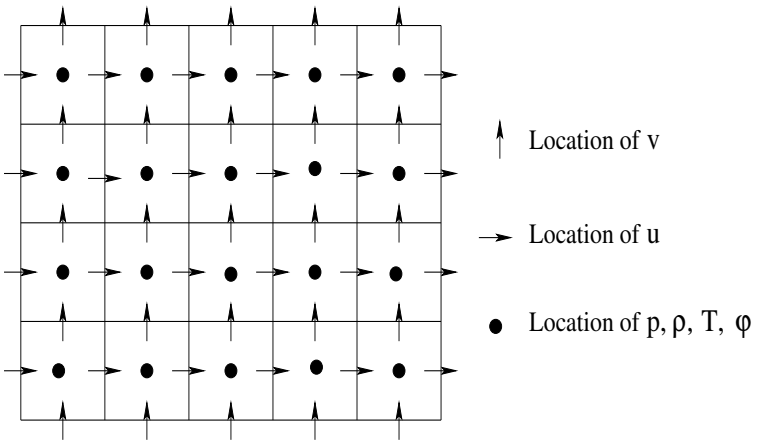

Figure 2: Staggered mesh used in the space discretization.

In order to formulate the fully discrete equations for the radiation hydrodynamic equations, we assume a uniform spatial mesh with grid sizes Δx and Δy in x- and y-direction, respectively. We also denote by w_{ij} the value of a function w at gridpoints (x_i, y_j). Therefore the Laplace operator in (3.1), (3.2), (3.4), (3.7) and (3.8) is discretized by the central differencing

$$\Delta w\Big|_{ij} \approx \frac{w_{i-1j} - 2w_{ij} + w_{i+1j}}{(\Delta x)^2} + \frac{w_{ij-1} - 2w_{ij} + w_{ij+1}}{(\Delta y)^2}.$$

The spatial derivatives of density in (3.5) are descretized by upwind differencing

$$\begin{aligned} u\frac{\partial \rho}{\partial x}\Big|_{ij} &\approx u_{ij}^{+}\frac{\rho_{ij} - \rho_{i-1j}}{\Delta x} + u_{ij}^{-}\frac{\rho_{i+1j} - \rho_{ij}}{\Delta x}, \\ v\frac{\partial \rho}{\partial y}\Big|_{ij} &\approx v_{ij}^{+}\frac{\rho_{ij} - \rho_{ij-1}}{\Delta y} + v_{ij}^{-}\frac{\rho_{ij+1} - \rho_{ij}}{\Delta y}, \end{aligned}$$

where

$$u_{ij}^{\pm} = \frac{1}{2}\left(u_{ij} \pm |u_{ij}|\right) \qquad \text{and} \qquad v_{ij}^{\pm} = \frac{1}{2}\left(v_{ij} \pm |v_{ij}|\right).$$

Due to the fact that at high Reynolds numbers the convective part in (3.8) becomes dominant, the spatial derivatives $\frac{\partial u^2}{\partial x}$, $\frac{\partial uv}{\partial y}$, $\frac{\partial uv}{\partial x}$ and $\frac{\partial v^2}{\partial y}$ in (3.8) have to be treated by a mixture of central and donor-cell differencing as in [20]. For instance, the derivative $\frac{\partial u^2}{\partial x}$ is approximated as

$$\begin{aligned} \frac{\partial u^2}{\partial x}\Big|_{ij} \approx\ & \frac{1}{\Delta x}\left(\left(\frac{u_{ij} + u_{i+1j}}{2}\right)^2 - \left(\frac{u_{i-1j} + u_{ij}}{2}\right)^2\right) + \\ & \frac{\delta}{\Delta x}\left(\frac{|u_{ij} + u_{i+1j}|\,(u_{ij} - u_{i+1j})}{4} - \frac{|u_{i-1j} + u_{ij}|\,(u_{i-1j} - u_{ij})}{4}\right), \end{aligned}$$

where $\delta \in [0, 1]$ is a chosen parameter, $\delta = 0$ corresponds to central differences and $\delta = 1$ yields the donor-cell differencing. The other spatial derivatives in the convective part of (3.8) can be handled similarly.

The full discrete formulation of the Poisson problem (3.9) is given by

$$\begin{aligned} &\frac{p_{i-1j}^{n+1} - 2p_{ij}^{n+1} + p_{i+1j}^{n+1}}{(\Delta x)^2} + \frac{p_{ij-1}^{n+1} - 2p_{ij}^{n+1} + p_{ij+1}^{n+1}}{(\Delta y)^2} - \frac{1}{\rho_{ij}^{n+1}}\frac{\rho_{i+1j}^{n+1} - \rho_{i-1j}^{n+1}}{2\Delta x}\frac{p_{i+1j}^{n+1} - p_{i-1j}^{n+1}}{2\Delta x} - \\ &\frac{1}{\rho_{ij}^{n+1}}\frac{\rho_{ij+1}^{n+1} - \rho_{ij-1}^{n+1}}{2\Delta y}\frac{p_{ij+1}^{n+1} - p_{ij-1}^{n+1}}{2\Delta y} = \frac{\rho_{ij}^{n+1}}{\Delta t}\left(\frac{u_{ij}^{\text{aux}} - u_{i-1j}^{\text{aux}}}{\Delta x} + \frac{v_{ij}^{\text{aux}} - v_{ij-1}^{\text{aux}}}{\Delta y} - Q_{ij}^{n+1}\right). \end{aligned} \tag{3.11}$$

At the boundary we use "ghost points" such that the boundary conditions enter the discrete equations via source terms and they are incorporated in the linear systems to be solved, compare [5] for more details. It is worth mentioning that the space and time discretizations presented in this paper are only first order accurate. In addition, to ensure stability of the solution procedure the time stepsize Δt has to satisfy the canonical hyperbolic and parabolic CFL conditions

$$u_{\max}\Delta t \leq \Delta x, \qquad v_{\max}\Delta t \leq \Delta y, \qquad \left(\frac{1}{(\Delta x)^2}+\frac{1}{(\Delta y)^2}\right)\frac{\Delta t}{Re} \leq \frac{1}{2}, \tag{3.12}$$

where $u_{\max} = \max_{ij}|u_{ij}|$ and $v_{\max} = \max_{ij}|v_{ij}|$.

4 Results and Numerical Examples

In this section we validate the models presented in this paper for two examples on fires in vehicular tunnels. As in [5], we consider two realistic fire events in a vehicle tunnel with length 1 km and 10 m height as well as a pressure difference (between top and bottom) of 120 Pa. The reference quantities and typical values suggested in [6] for fires in vehicle tunnels are listed in table 1. A heat source with area size of 10 $m \times 4$ m and strength of 10 MW is located in the middle of the tunnel. Here the heat source is implemented as an indicator function and not as an obstacle. The radiation source in the temperature equation is acting on the whole domain. Initially, we set the following conditions

$$u(t=0,x,y) = v(t=0,x,y) = 0, \qquad \rho(t=0,x,y) = 1.2, \qquad p(x,y) = \rho g y,$$

which correspond to a fluid at rest with hydrostatic pressure. All linear systems are solved using the preconditioned BiCGStab algorithm with a tolerance of 10^{-7} to stop the iterations. The total duration of simulation is 20 min. In all our simulations we use variable time stepsizes Δt adjusted at each step according to (3.12) as

$$\Delta t = C \min\left(\frac{\Delta x}{u_{\max}}, \frac{\Delta y}{v_{\max}}, \frac{Re}{2}\left(\frac{1}{(\Delta x)^2}+\frac{1}{(\Delta y)^2}\right)^{-1}\right),$$

where C is a safety factor set to $1/2$ for all test cases to ensure the stability of the numerical scheme. We assume non-scattering and gray participating media in the tunnel. Thus the black-body radiation is given by

$$B(T) = a_R T^4,$$

where $a_R = 5.67 \times 10^{-8}$ W/m^2K^4 is the Boltzmann constant. The spatial domain is discretized into 2500×50 gridpoints and the optical scale is $\tau = 0.1$. We should mention that non-gray computations can also be carried out using our simplified models provided detailed information on the spectral properties of the medium is given. In the sequel we shall use the terminology SP_0, SP_1, and SP_3 to refer to the equations (2.15), (2.15)-(2.18) and (2.15)-(2.19), respectively. Two situations are selected namely fire accidents in a tunnel without slope and in a tunnel with slope of 3%.

4.1 Vehicular Tunnel without Slope

Our first test example is a fire event in vehicular tunnel without slope. The isotherm plots obtained by the SP_0, SP_1 and SP_3 models are shown in figure 3 at different times. In each case the fluid rises from the hot source and propagates along the cold regions in the tunnel as can be clearly seen in figure 4, where temperature distribution is plotted together with velocity vectors obtained by

Table 1: Quantities, units, reference quantities and typical values used in computations.

Quantity	Unit	Reference quantity	Typical reference value
t	s	$t_\infty = u_\infty/h$	$15\ min$
x, y	m	L	$10^3 - 10^4\ m$
height	m	h	$10\ m$
u	m/s	u_∞	$1\ m/s$
ρ	kg/m^3	ρ_∞	$1.2\ kg/m^3$
p	kg/ms^2	p_∞	$10^5\ Pa = 10^5\ kg/ms^2$
f	m/s^2	f_∞	$10\ m/s^2$
T	K	T_∞	$300\ K$
σ	$1/m$	σ_∞	$1\ /m$
κ	$1/m$	κ_∞	$100\ /m$
I	$kg/s^3\ sr$	I_∞	$1\ kg/s^3\ sr$
q	W/m^3	q_∞	$10^5 - 10^6\ W/m^3$
R	m^2/Ks^2		$287\ m^2/Ks^2$
c_p	m^2/Ks^2		$1005\ m^2/Ks^2$
λ	kgm/Ks^2		$25 \cdot 10^{-3}\ kgm/Ks^2$
μ	kg/ms		$18 \cdot 10^{-6}\ kg/ms$

the SP_3 approximation. The results obtained by SP_0 and SP_1 approximations are not included in this figure for sake of brevity. The absence of pressure differences between the entrance and exit of the tunnel permits to the temperature fronts to move symmetrically with respect to the middle of the tunnel where the source is located. Some deviations on the temperature plots between the left and right regions are observed in the horizontal cross sections in figure 6, which may be caused by the coarse mesh used in the simulations.

In order to have a clear comparison between the nonradiating convection (SP_0 model) and the radiating convection (SP_1 and SP_3 models), we display in figure 5 vertical cross sections of the computed temperatures at two points in the tunnel. The first point is located exactly at the source position, while the second point is positioned at 100 m right from the source. The horizontal cross sections of the computed temperature in the middle of tunnel height are presented in figure 6 at four different instants. As can be seen from these figures, the maximum temperature occurs in the source region, which explains why the fluid rises in the central region of the tunnel and moves symmetrically downstream and upstream. For instance, in the point located at $(600\ m, 5\ m)$, the maximum value of the temperature predicted by SP_3 approximation is 3.4% higher than SP_0 results at time $t = 4\ min$, while at time $t = 16\ min$, the SP_3 temper! ature is 5.2% higher than SP_0 temperature.

The time evolutions of the temperature for two points located at $(500\ m, 5\ m)$ and $(600\ m, 5\ m)$ are presented in figure 7. The difference in accuracy between SP_1 and SP_3 results were not significant, which confirms the asymptotic expansion discussed in section 2.2. Here the fluid radiation increases with fluid temperature and when the fluid temperature is less than 700 K, combined radiation and convection is close to pure convection. When radiation is included, temperature decreases near the fire event and increases in regions far from the source. This can be explained as follows. A radiative energy is proportional to the fourth power of absolute temperature, with the increase of temperature difference the radiative heat transfer between the hot source and the

closer regions becomes stronger than that between the other cold regions in the tunnel. On the other hand, the temperature gradients are weakened near the hot source but strengthened n! ear the far cold regions.

4.2 Vehicular Tunnel with 3% Slope

The second test example consists of a fire event in vehicular tunnel with a slope of 3%. We use the same setting as the previous example. This test case occurs in many realistic fire events and differs from the previous example in that, in the current example, pressure differences are present in the tunnel and buoyancy effects act as additional forces. In figure 8 we present the isotherms plots obtained by the SP_0, SP_1 and SP_3 models at different times. Temperature distributions and velocity vectors obtained by the SP_3 model are shown in figure 9. It is clear that the slope strongly alters the distribution of fluid temperature in the tunnel and also breaks the symmetry detected in the case with vanishing slope. Initially the flow field and temperature propagate downstream (entrance) in the tunnel, after certain time the flow moves upstream (exit) in the tunnel as can be seen from figure 8 and fig! ure 9. This is due to buoyancy forces acting in the tunnel with slope. Similarly to the previous example there is no significant differences between the SP_1 results and those obtained by the SP_3 model.

Overall the temperature levels for radiating fluid (SP_1 and SP_3 models) are lower and more uniform than for the nonradiating fluid (SP_0 model) as radiation provides an additional mechanism to transfer the heat generated inside the tunnel. As a consequence, the flow near the heated source breaks down and weakens considerably. As expected, in the region near the fire source, a strong heat transport induced by the pressure difference and therefore much lower temperatures are predicted.

Figure 10 shows the time evolution of the temperature for two points located near the fire source at $(540\ m, 0.4\ m)$ and $(540\ m, 0.8\ m)$, respectively. As discussed in the previous example, the radiating SP_1 and SP_3 models generally overpredict the velocities, especially those in the neighboring regions to the heat source. When the radiative participation is more important, velocity increases in the fire source. Therefore mass transport is more important in the center of the tunnel. Thus this center participates more in transfers, as shown from the results presented in figure 9. Furthermore, the appearance of radiation varies the temperature distribution in the tunnel, so that the temperature and the flow field in the tunnel are altered. For example, in the point located at $(540\ m, 0.4\ m)$, the maximum value of the temperature predicted by SP_3 approximation is 2.1% higher than SP_0 results at time $t = 4\ min$. At time $t = 16\ min$, ! this percentage changes to 3.7%.

As a final remark we want to comment on the computational work for the presented approximations. The number of iterations and CPU times required by SP_0 approximation solutions were but slightly lower than the respective SP_1 solutions. The SP_3 approximation, which is comparable to the discrete ordinates method in accuracy [17], requires simultaneous solution of two second-order elliptic differential equations for radiation calculations compared to one elliptic equation for the SP_1 approximation.

5 Conclusions

In this paper we have presented a comprehensive methodology for realistically predicting thermal flows at low Mach number. The flow equations are derived from a low-Mach asymptotic in the compressible Navier-Stokes problem. The radiation is approximated by the SP_N equations also derived by an asymptotic expansion in the radiative transfer problem. The combined models have the potential to eliminate many difficulties that one faces when attempting to solve the radiation hydrodynamic equations. For example, the low-Mach asymptotic removes the acoustic waves from

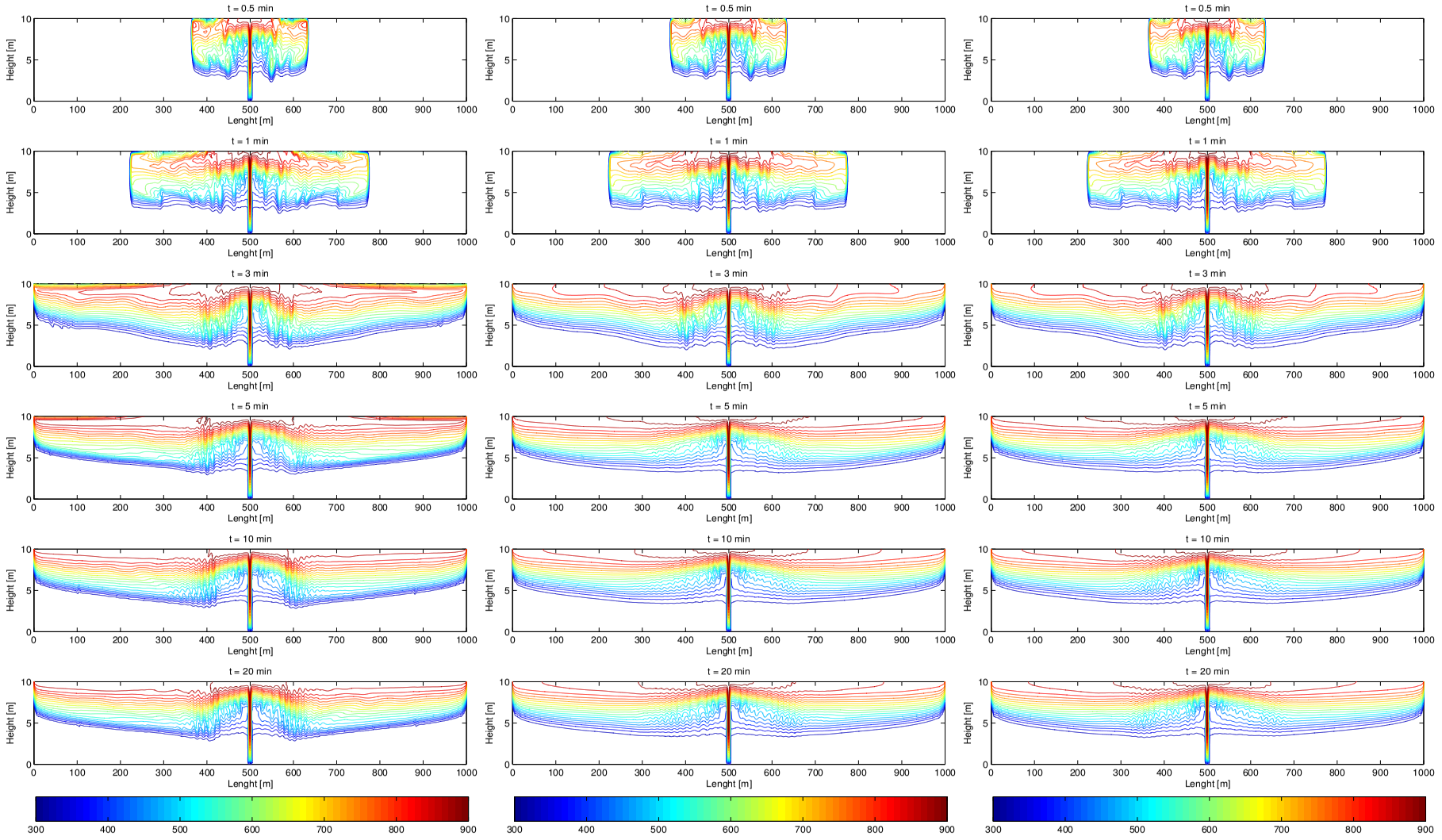

Figure 3: Isotherms for SP_0 (left column), SP_1 (middle column) and SP_3 approximations (right column) for the tunnel without slope.

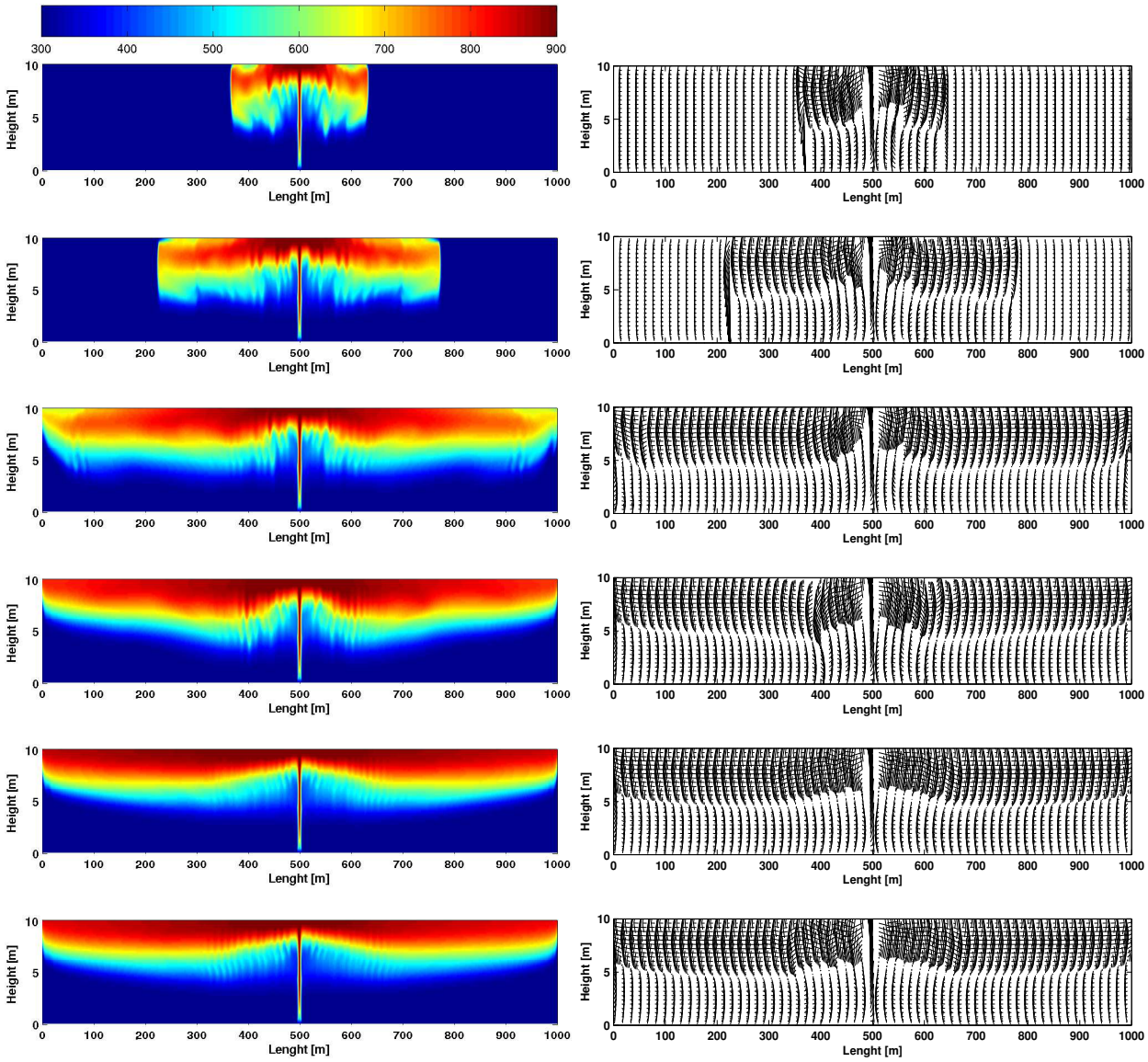

Figure 4: Temperature distribution and velocity vectors obtained by SP_3 approximation for the tunnel without slope at times $t = 0.5$, 1, 2, 3, 5, 20 *min*.

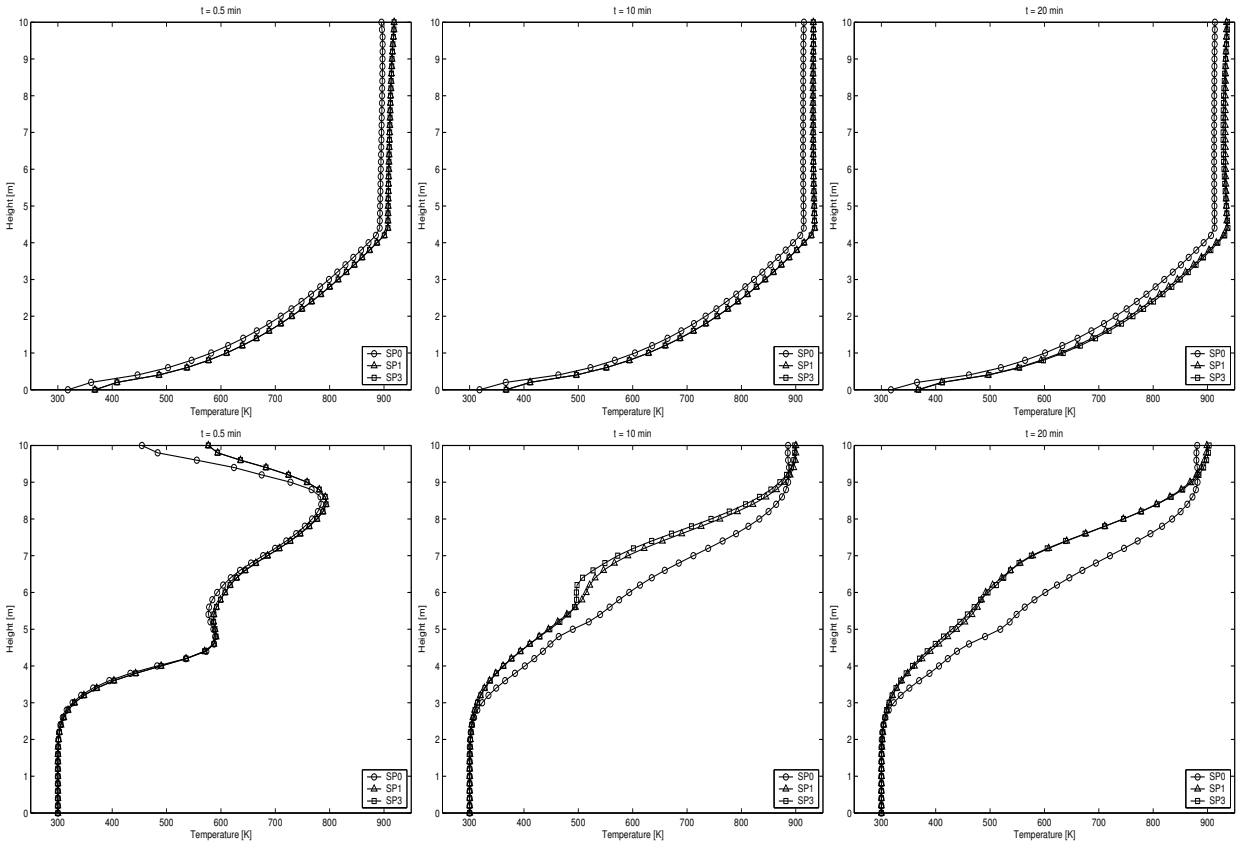

Figure 5: Vertical cross sections of the temperature at $x = 500\ m$ (top row) and at $x = 600\ m$ (bottom row) in the tunnel without slope.

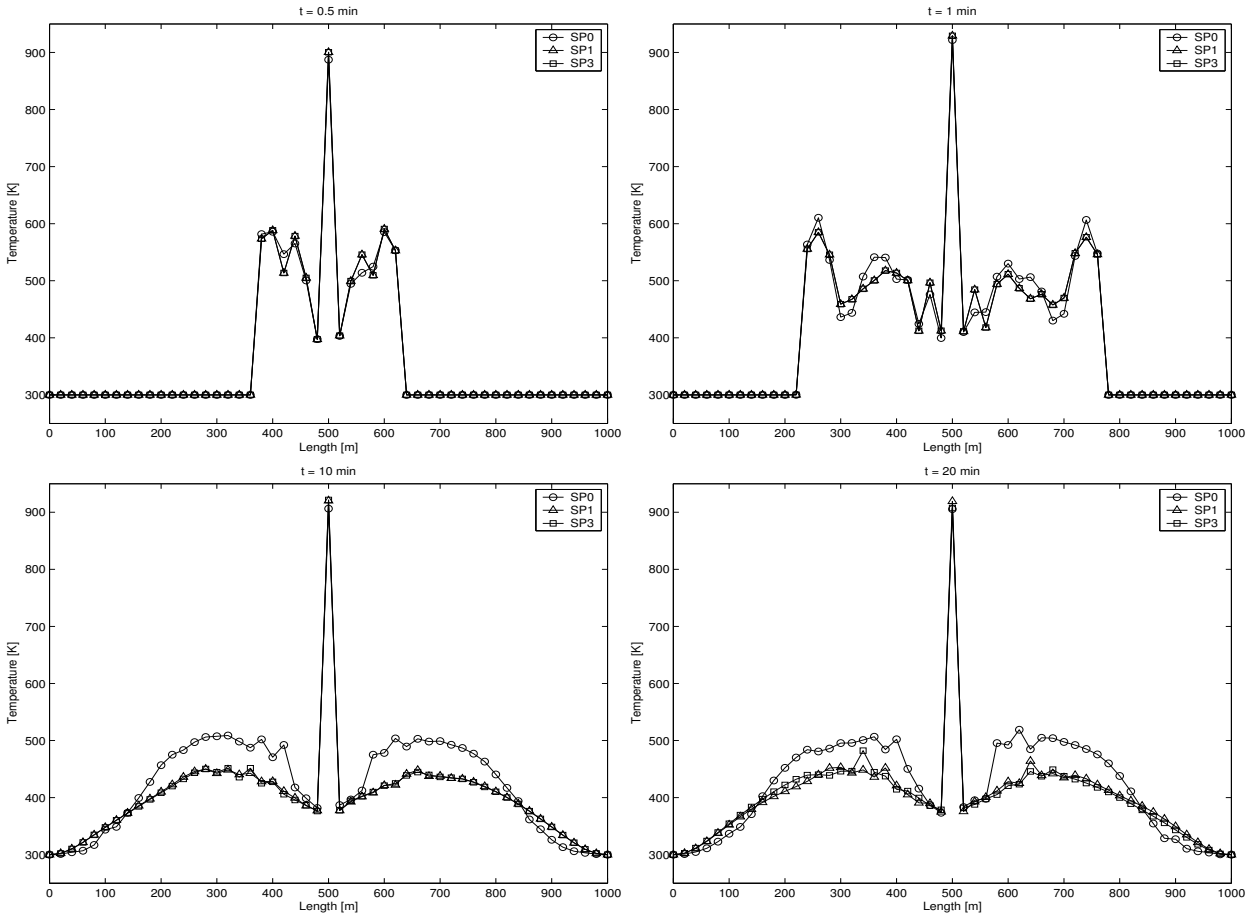

Figure 6: Horizontal cross sections of the temperature at $y = 5\ m$ for different times.

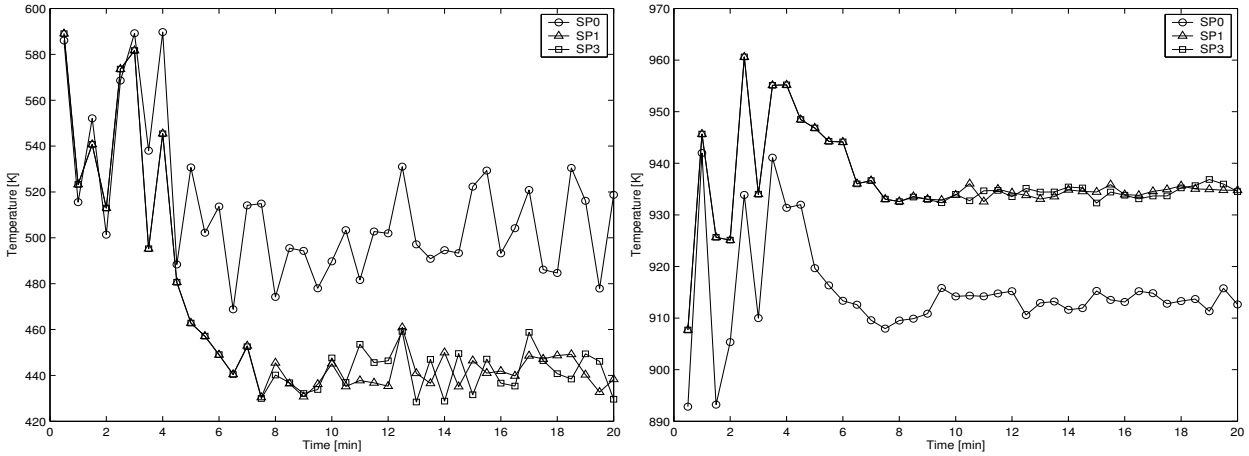

Figure 7: Time evolution of the temperature for points located at $(500\ m, 5\ m)$ (left column) and at $(600\ m, 5\ m)$ (right column) in the tunnel without slope.

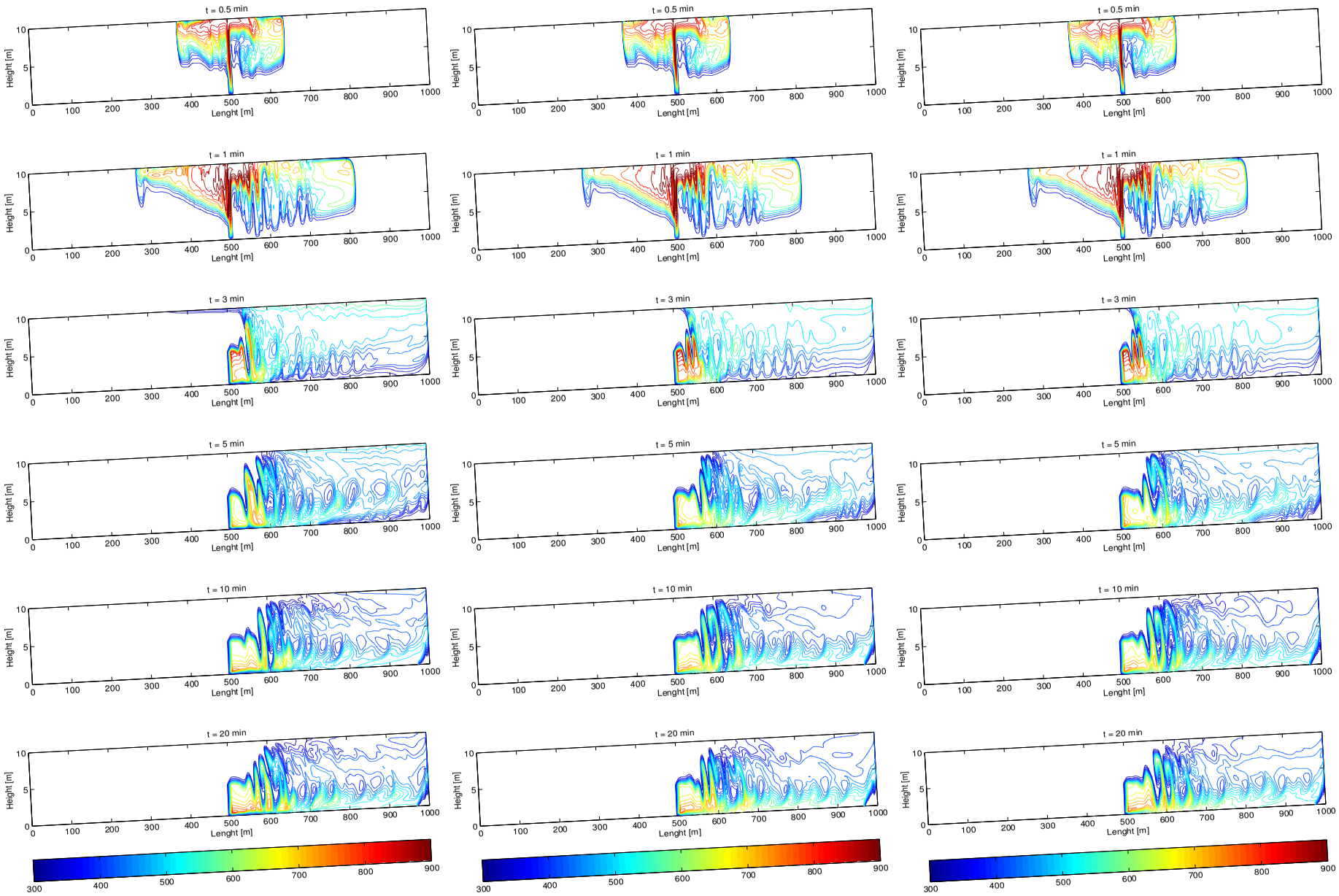

Figure 8: Isotherms for SP_0 (left column), SP_1 (middle column) and SP_3 approximations (right column) for the tunnel with 3% slope.

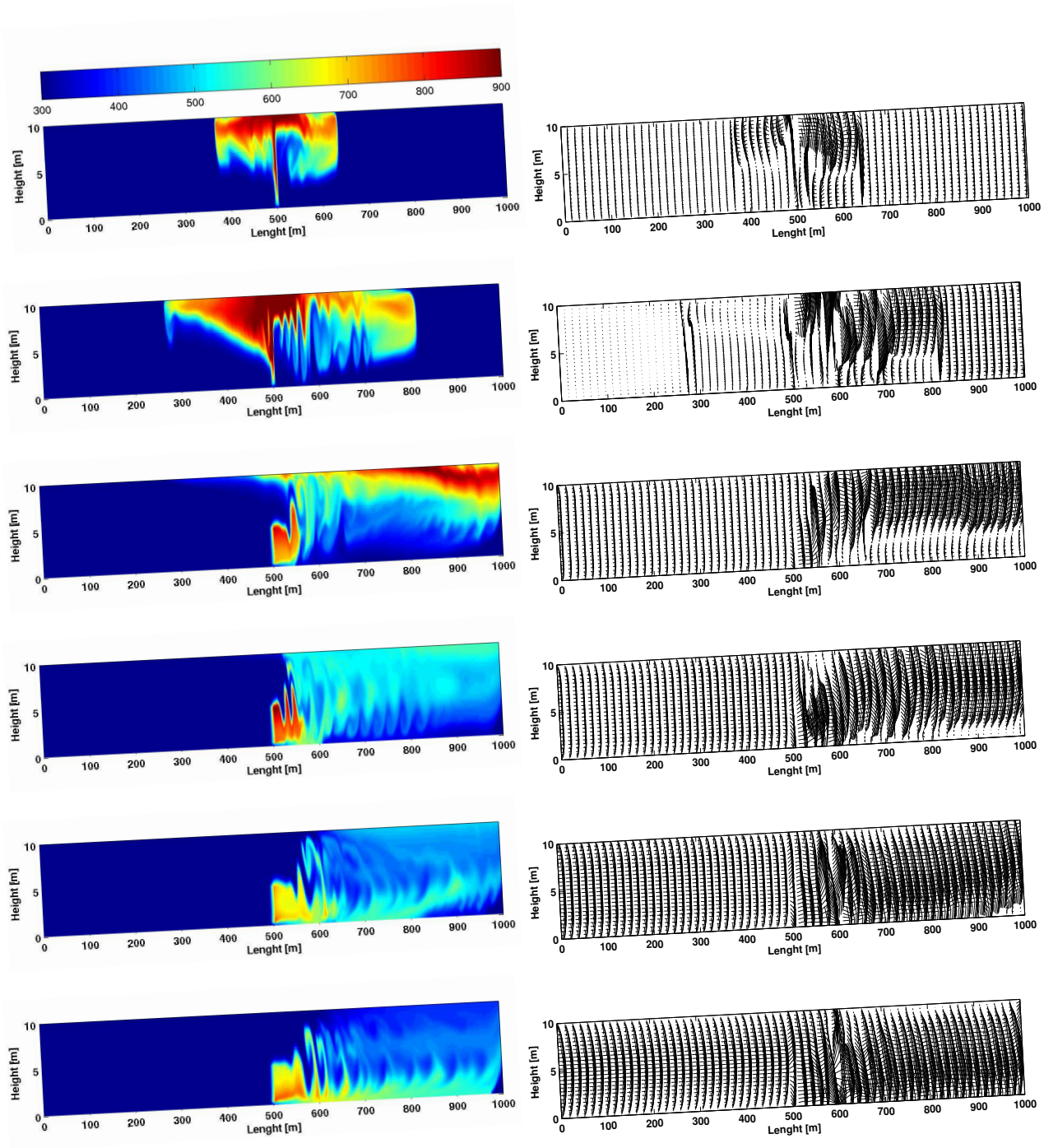

Figure 9: Temperature distribution and velocity vectors obtained by SP_3 approximation for the tunnel with a slope at times $t = 0.5,\ 1,\ 2,\ 3,\ 5,\ 20\ min$.

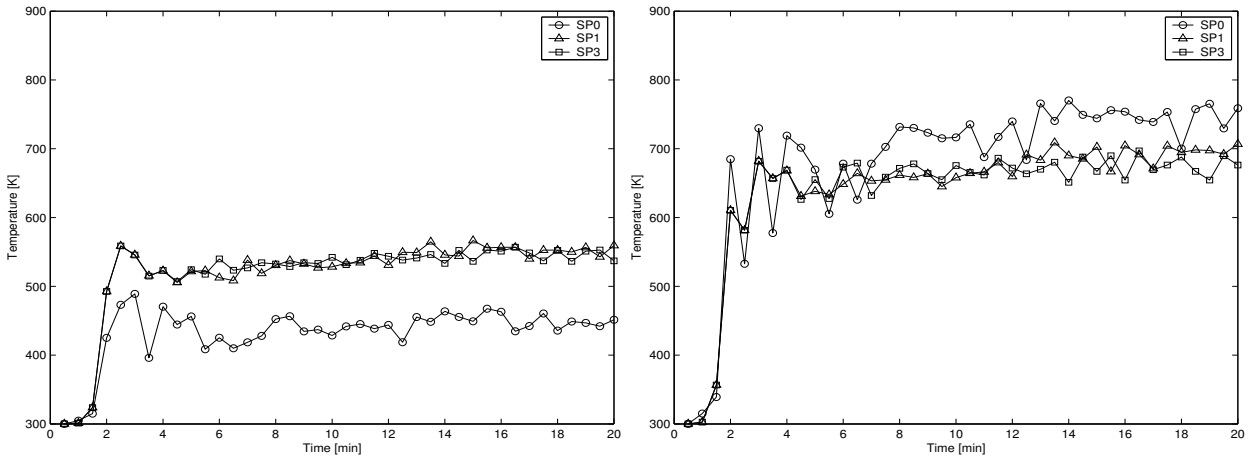

Figure 10: Time evolution of the temperature for points located at (540 $m, 0.4$ m) (left column) and at (540 $m, 0.8$ m) (right column) in the tunnel with 3% slope.

the compressible flow without eliminating density variation. Whereas, the $\mathrm{SP_N}$ approximations for radiative transfer result in a set of equations independent of directional coordinates and easy to solve. To solve the proposed models numerically we have implemented a modified MAC method that allows incorporation of radiation source terms. Results indicate that the models are efficient in generating accurate solu! tions and prove to be strong candidates for the integration into comprehensive software packages.

Validation of the models has been carried out using two fire events in vehicular tunnels. In the first example, the tunnel is without slope which ensures that no pressure differences take place in the tunnel. The second example assumes a tunnel with a slope of 3% which allow buoyancy forces to act in the tunnel. In both examples the heat source is centered in the tunnel and has a strength of 10 MW corresponding to a burning car. It has been shown that for low temperatures, fluid radiation does not strongly affect the convective heat transfer. However, if the radiative term is much higher than the convective term, this conclusion may not hold. A large heat flux gradient can change the temperature gradient, which will affect convective heat transfer. Furthermore, in both examples the corresponding flow fields are affected by the presence of radiation. For instance, velocities are intensified in regions near the fire source.

Although the new models were successfully implemented in a realistic fire event in tunnels, before recommending a final version for widespread industrial two issues need to be considered. First, real Reynolds numbers and chemical reactions in the fire event which have the advantage of predicting turbulence effects. Second, revisiting the gray assumption by consider the optical properties of mixed gases in the tunnel. These and further issues are subject of future investigations.

References

[1] R. Backofen, T. Bilz, A. Ribalta and A. Voigt, *SP_N-Approximations of Internal Radiation in Crystal Growth of Optical Materials*, *J. Crystal Growth.* **266** (2004) 264–270.

[2] W. Fiveland, *The Selection of Discrete Ordinate Quadrature Sets for Anisotropic Scattering*, *ASME HTD. Fundam. Radiat. Heat Transfer.* **160** (1991) 89–96.

[3] M. Frank, M. Seaïd, J. Janicka, A. Klar, R. Pinnau and G. Thömmes, *A Comparison of Approximate Models for Radiation in Gas Turbines*, *Int. J. Progress in CFD.* **3** (2004) 191–197.

[4] E.M. Gelbard, *Simplified Spherical Harmonics Equations and their Use in Shielding Problems.* Technical Report WAPD-T-1182, Bettis Atomic Power Laboratory, 1961.

[5] I. Gasser, J. Struckmeier and I. Teleaga, *Modelling and Simulation of Fires in Vehicle Tunnels*, *Int. J. Numer. Methods Fluids.* **44** (2004) 277–296.

[6] I. Gasser and J. Struckmeier, *An Asymptotic Induced One-Dimensional Model to Describe Fires in Tunnels*, *Mathematical Modelling in Applied Sciences.* **25** (2002) 1231–1249.

[7] F. Harlow and J. Welch, *Numerical Calculation of Three Dependent Viscous Incompressible Flow of Fluid with Free Surface*, *Physics of Fluids.* **8** (1965) 2182–2189.

[8] A. Klar, J. Lang and M. Seaïd, *Adaptive Solutions of* $\mathrm{SP_N}$ *-Approximations to Radiative Heat Transfer in Glass*, *Int. J. Thermal Sciences.* (2005) to appear

[9] G. Lauriat, *Combined Radiation-Convection in Gray Fluids Enclosed in Vertical Cavities*, *J. Heat Transfer.* **104** (1982) 609–615.

[10] Liu, F., H. Becker, and Y. Bindar, *A Comparative Study of Radiative Heat Transfer Modelling in Gas-Fired Furnaces using the Simple Grey gas and the Weighted-sum-of grey-gases Models*, *International Journal Heat and Mass Transfer.* **41** (1998) 3357–3371.

[11] E. Larsen, G. Thömmes, A. Klar, M. Seaïd and T. Götz, *Simplified* P_N *Approximations to the Equations of Radiative Heat Transfer and Applications*, *J. Comp. Phys.* **183** (2002) 652–675.

[12] E. Larsen, J. Morel and J. McGhee, *Asymptotic Derivation of the Multigroup* P_1 *and Simplified* P_N *Equations with Anisotropic Scattering*, *Nucl. Sci. Eng.* **123**(1996) 328–367.

[13] M. Majda and J. Sethian, *The Derivation and Numerical Solution of the Equations for Zero Mach Number Combustion*, *Combustion Science and Technology.* **42**(1985) 185–205.

[14] D. Mihalas and B. S. Mihalas, *Foundations of Radiation Hydrodynamics.* Oxford University Press, New York, 1983.

[15] M. F. Modest, *Radiative Heat Transfer.* McGraw-Hill, 1993.

[16] M. Seaïd, A. Klar and R. Pinnau, *Numerical Solvers for Radiation and Conduction in High Temperature Gas Flows*, *J. Flow Turbulence and Combustion.* (2005) to appear

[17] M. Seaïd, M. Frank, A. Klar, R. Pinnau and G. Thömmes, *Efficient Numerical Methods for Radiation in Gas Turbines*, *J. Comp. Applied Math.* **170** (2004) 217–239.

[18] G. Thömmes, R. Pinnau, M. Seaïd, T. Götz and A. Klar, *Numerical Methods and Optimal Control for Glass Cooling Processes*, *Transp. Theory Stat. Phys.* **31** (2002) 513–529.

[19] N. Selçuk and N. Kayakol, *Evaluation of Discrete Ordinates Method for Radiative Transfer in Rectangular Furnaces*, *International Journal Heat and Mass Transfer.* **40** (1997) 213–222.

[20] M. Tom, S. McKee Gensmac, *A Computational Marker and Cell Method for Free Surface Flows in General Domains*, *J. Comp. Phys.* **110** (1994) 171–186.

[21] E. Turkel, R. Radespiel, N. Kroll, *Assessment of Preconditioning Methods for Multidimensional Aerodynamics*, *Computer & Fluids*, **26** (1997) 613–634.

[22] H. A. van der Vorst, *BI-CGSTAB: A Fast and Smoothly Converging Variant of BI-CG for the Solution of Nonsysmmetric Linear Systems*, *SIAM J. Sci. Statist. Comp.* **13** (1992) 631–644.

[23] J. Welch, F. H. Harlow, J. P. Shannon, B. J. Daly *The MAC Method a Computing Technique for Solving Viscous, Incompressible, Transient Fluid-Flow Problems Involving Free Surfaces*, *Los Alamos Scientific Laboratory California*, **LA-3425** (1966).